Determination of the X-Auger electron spectroscopy evolution of indium in InSb by linear and nonlinear least squares approaches

Solène Béchu, Neal Fairley

Determination of the X-Auger electron spectroscopy evolution of indium in InSb by linear and non-linear least squares approaches

Solène Béchu [1, a)], Neal Fairley [2]

[1]Institut Lavoisier de Versailles (ILV), Université de Versailles Saint-Quentin-en-Yvelines, Université Paris-Saclay, CNRS, UMR 8180, 45 avenue des Etats-Unis, 78035 Versailles Cedex, France.
[2]Casa Software Ltd, Bay House, 5 Grosvenor Terrace, Teignmouth, Devon TQ14 8NE, UK

[a)] Electronic mail: solene.bechu@uvsq.fr

X-ray photoelectron spectroscopy (XPS) is a major and valuable chemical analysis technique that can bring a wide range of information if one takes time to carefully interpret the spectra. In particular, many metrological developments deal with the modeling of photoelectron peaks while X-Auger transitions still remain hardly exploited. Here, an innovative approach examining in a complementary way these spectral features is presented and illustrated on concrete case dealing with the chemical changes of indium in the InSb semiconductor during its air aging. Indium contains an extensive range of photopeaks along the energy scale, meaning electrons emitted from different escape depths are present on a same widescan spectrum and thus, information from different depths are accessible. Specifically, this study focuses on indium's X-Auger electron spectroscopy (X-AES) transitions and decomposition to track the outer surface chemistry evolution of the InSb semiconductor. To this end, we compared linear and nonlinear least-squares approaches to decompose the In $M_{4,5}N_{4,5}N_{4,5}$ X-AES transition and demonstrate the oxide growth progression. For both approaches, we applied the vectorial method (also known as the informed amorphous sample model) to retrieve the different chemical environments present during air aging. Linear and nonlinear least-squares approaches were both found to

yield comparable results, with a comparative error of less than 10%. Over time, a progressive growth of the oxide layer was demonstrated, ranging from 0.3 ± 0.2 to 2.9 ± 0.2 nm using the X-AES transitions. Additionally, the decomposition of the In 3d and In 4d photoelectron peaks showed a lower thickness of oxide with time, due to the lesser surface sensitivity of these peaks.

I. INTRODUCTION

III-V semiconductors play a crucial role in everyday life and find extensive usage in various applications including photovoltaic cells,[1,2] electronic and optoelectronic devices.[3] To control, optimize and prevent the deviation of semiconductor properties, it is necessary to acquire a better understanding of the semiconductor aging behavior, at different time scales, ranging from minutes to days of exposure. The detection of the initial degradation relates to the reactivity of the semiconductor surface and an appropriate analysis tool. Surface analysis is a valuable technique to understand the degradation mechanisms, particularly during the initiation phase. X-ray photoemission spectroscopy (XPS), being both quantitative and non-destructive, is an ideal analytical tool to investigate the aging process of materials. Moreover, XPS is surface-sensitive and offers insights into chemical environments, enhancing the understanding of chemical evolution. It has been extensively used to evaluate various materials and is a reliable method for fine chemical characterization.[4–7] This technique is commonly used, but there is still valuable information that has yet to be explored, especially for the semiconductors based on In, such as InSb.

Using an Al Kα source (1486.6 eV), several indium photoelectrons can be detected over a wide kinetic energy range, including: In 3s (666 eV), In $3p_{1/2}$ (784 eV), In $3p_{3/2}$ (822 eV), In $3d_{3/2}$ (1035 eV), In $3d_{5/2}$ (1043 eV), In 4s (1364 eV) and In 4d (1470 eV), in kinetic energies (KE). However, since there are no photopeaks for kinetic energies below 600 eV, obtaining information from the outer surface becomes impossible when angle resolved XPS cannot be performed.[8] Therefore, analyzing the In $M_{4,5}N_{4,5}N_{4,5}$ X-Auger electron spectroscopy (X-AES) transitions (located around 400 eV, KE) is a good alternative to get complementary information and to lower the detection threshold of indium oxide. In the literature, X-AES transitions are primarily utilized to calculate the modified Auger parameter, leading to better identification of an element's chemical state.[9] The calculation of the modified Auger parameter does not require any fitting procedure, and solely entails obtaining the position of the corresponding X-AES transition. Except for the modified Auger parameter, the use of X-AES lines is not very widespread. Only a small number of papers have addressed this topic,[10–13] with even fewer providing the fitting procedure.[14,15] Interestingly, two different modeling approaches can be utilized for fitting X-AES lines. The first approach illustrated by Biesinger *et al.*[15] is based on a non-linear least square method. It was illustrated on a mixture of Cu oxides to determine, from the Cu $L_3M_{4,5}M_{4,5}$ lines fitting, its exact composition. The non-linear least square method[16] consists of searching for a set of parameters (such as Gaussian or Lorentzian curves) that provide a solution for fitting the curves to the data. This method allows for the adjustment of the parameters based on any potential changes in the chemical environment, such as FWHM parameter (Full Width at Half-Maximum). Each chemical environment envelop can be modeled by one or more Gaussian/Lorentzian contributions, which can consequently

complexify the fitting. It is the most widely used fitting procedure in XPS analysis.[17] In contrast, Iwasaki *et al.*[14] conducted a linear least square fitting of In $M_{4,5}N_{4,5}N_{4,5}$ X-AES lines for an InSb sample. The linear least square method relies on the summation of fixed components (here In $M_{4,5}N_{4,5}N_{4,5}$ envelops) to create a parametric curve. It results thus in a unique optimal set of parameters, for a given set of component curves and data.[18] This technique permits the use of intricate spectral shapes like X-AES lines, whereby data modeling is feasible using spectral shapes sources from within a data set or standard samples. Both measured or derived spectral shapes should be considered as guidelines for selecting appropriate line shapes for components in a peak model.[19] In this study, to evaluate the pros and cons of these two approaches, they will both be applied for the aging study of InSb, to model In $M_{4,5}N_{4,5}N_{4,5}$ X-AES transitions.

Since X-AES spectra are expected to progressively evolve in time, it is crucial to establish the number of spectral shapes that represent the actual chemical species. Space dimension determination using abstract factors through PCA (Principal Component Analysis) can solve this problem.[20–24] Upon determining the number of chemical species, it is necessary to establish their respective spectral forms. The challenge that may arise at this stage is the accurate definition of chemical states. In fact, the evolution of the X-AES spectra may sometimes not directly provide access to the spectral shape of the individual chemical states involved. To resolve this problem, weighted differences on a set of evolving data to acquire mathematical vectors that represent inherent chemical states can be performed. This method, known as the informed amorphous sample model or vectorial method, has been successively applied to photoemission and infrared data,[19,25,26] and will

be implemented on our In $M_{4,5}N_{4,5}N_{4,5}$ X-AES transitions dataset of spectra acquired on InSb until 270 hours air aging.

The combination of non-linear and linear fitting procedures, space dimension determination and the vectorial method will be utilized to examine how the In XPS signal evolves across a broad range of kinetic energies (attainable from an Al Kα source) during the aging of the InSb semiconductor. The gradual oxidation front of indium within the InSb semiconductor will be revealed *via* the combination of various photopeaks and X-AES transitions and a comparison with the evolution of the antimony chemical environment will also be conducted.

II. EXPERIMENTAL

A. Materials

The InSb p-doped substrate was purchased from El Cat Inc. and In_2O_3 was obtained naturally through the aging of metallic In. Prior to the XPS measurements, InSb was deoxidized in 3 M HCl (37%, ACS grade, from SUPELCO) for 5 minutes and was subsequently rinsed using deionized water (18 mΩ) and dried under N_2 flux. To limit the inherent oxidation, the sample was mounted for XPS analysis within a glovebox.

The InSb sample underwent sequential aging in ambient air, under ambient light, at a controlled temperature of 20°C and relative humidity of 60%. The XPS measurements were taken after 0.5, 1, 2, 3, 4, 5, 150, 220 and 270 hours of air exposure.

B. Methods

XPS surface chemical analyses were performed on a Thermo Scientific Nexsa™ spectrometer equipped with a monochromatic Al-Kα X-ray source (1486.6 eV). The

Thermo Electron procedure was used to calibrate the Nexsa spectrometer using metallic Cu and Au samples as internal references (Cu $2p_{3/2}$ at 932.6 eV and Au $4f_{7/2}$ at 84.0 eV). High energy resolution spectra were acquired using an X-ray spot size of 400 μm, using a constant analyzer energy (CAE) mode of 20 eV, 0.1 eV as the energy step size and a dwell time of 100 ms. X-AES lines were examined using a CAE mode of 50 eV, an energy step size of 0.1 eV and a dwell time of 100 ms. Charge neutralization was not applied to the sample due to its nature.

C. Data processing

Data were processed with the CasaXPS software (version 2.3.25), using the Al-Thermo-1 library. Samples were recalibrated using the binding energy of the chemical environment of In in InSb for the In $4d_{5/2}$ photopeak (17.4 eV),[27] and the chemical environment of In in In_2O_3 for the In $3d_{5/2}$ photopeak (444.8 eV).[28]

In 3d and In 4d spectra were processed using a Shirley background and a convolution of Gaussian Lorentzian (LA(85)) peak shapes for the In 3d and In 4d photopeaks. For the X-AES transitions, U 2 Tougaard backgrounds were applied, while a combination of convolution Gaussian Lorentzian peak shapes (LA(30)) was utilized for the non-linear least square decomposition.

The space dimension was determined by calculating abstract factors (Options/Processing/PCA), and applied to the initial and final spectra of the In $M_{4,5}N_{4,5}N_{4,5}$ transitions using 12 factors. The vectorial method (weighted differentiation, available in Options/Processing/Calculator) was applied to the initial and the final X-AES lines of In $M_{4,5}N_{4,5}N_{4,5}$, using the following equation:

$$X_j = (1 - c_j)S_i - c_j S_f \qquad \text{Equation 1}$$

Where X_j is the mathematical vector, c_j is the weighted factor that varies between 0 and 1 with a step of 0.1, S_i, the initial spectrum and S_f, the final spectrum.

The oxide film thickness was calculated using the formula developed by Strohmeier and Carlson[29,30] as defined by the following equation:

$$d = \lambda_{ox} \sin\theta \ln\left(\frac{N_{sc}\lambda_{sc}I_{ox}}{N_{ox}\lambda_{ox}I_{sc}} + 1\right) \qquad \text{Equation 2}$$

Where d is the thickness defined in Å, θ, the photoelectron take-off angle (90°), λ_{ox} and λ_{sc} the inelastic mean free paths (IMFP, λ in Å) of the oxide and the semiconductor, I_{ox} and I_{sc}, , the area percentages of the oxide and semiconductor photopeaks from the high-resolution spectrum, and N_{ox} and N_{sc}, the volume densities of the atoms in the oxide and semiconductor phases, respectively.

The IMFP values of the electrons at different kinetic energies were calculated with the QUASES-IMFP-TPP2M version 3.0 software using the TPP-2M formula and are shown in Table 1.

TABLE 1. IMFP values for the different chemical environments.

KE of emitted photoelectrons (eV)	Transition	λ_{InSb} (Å)	$\lambda_{In_2O_3}$ (Å)	$\lambda_{Sb_2O_5}$ (Å)	InSb depth probed (nm)	In_2O_3 depth probed (nm)	Sb_2O_5 depth probed (nm)	$N_{In_2O_3}$	N_{InSb}	$N_{Sb_2O_5}$
1468	In 4d	33.88	24.04	/	10	7	/	7.18	5.78	/
1042	In $3d_{5/2}$	25.93	18.50	/	8	6	/			
408	In $M_4N_{4,5}N_{4,5}$	13.10	9.52	/	4	3	/			
1454	Sb 4d	33.67	/	28.45	10	/	9	/		3.78
958	Sb $3d_{5/2}$	24.38	/	20.54	7	/	6			

III. RESULTS AND DISCUSSION

A. Decomposition of the In $M_{4,5}N_{4,5}N_{4,5}$ X-AES lines during air aging

During ambient aging of the InSb semiconductor, its surface evolution is regularly monitored by XPS measurements. As electrons from the In $M_{4,5}N_{4,5}N_{4,5}$ X-AES lines are emitted from a kinetic energy range of 390 eV to 415 eV, their escape depths are in the order of 3 to 4 nm (Table 1) conferring them a higher sensitivity to the outer surface. These electrons are expected to be the initial ones to interact with the surrounding environment throughout the aging process. Therefore, they depict the fastest increase of a new contribution relative to the In_2O_3 environment. Thus, we will first consider the tracking of the evolution of the In $M_{4,5}N_{4,5}N_{4,5}$ X-AES transitions.

1. In $M_{4,5}N_{4,5}N_{4,5}$ X-AES reference spectra for InSb and In_2O_3 environements

Fig. 1 a. shows the In $M_{4,5}N_{4,5}N_{4,5}$ X-AES lines for InSb, at t_0 and after 270 hours of aging. Regarding the InSb spectrum at t_0, the main In $M_4N_{4,5}N_{4,5}$ transition is located at 408.8 eV ± 0.1 eV, KE, and the main In $M_5N_{4,5}N_{4,5}$ line at 401.3 ± 0.1 eV, KE. The modified Auger parameter α'= KE (In $M_4N_{4,5}N_{4,5}$)+BE (In3 $d_{5/2}$) reaches thus the typical InSb environment value of 853.2 ± 0.2 eV.[9] After 270 hours of aging, changes are observed, through the appearance of new transition lines at higher kinetic energies. The main In $M_4N_{4,5}N_{4,5}$ X-AES line is specified at 405.4 eV ± 0.1 eV, KE, and the main In $M_5N_{4,5}N_{4,5}$ transition at 398.1 ± 0.1 eV, KE. Here, the modified Auger parameter value of 850.7 ± 0.2 eV confirms the chemical environment of In_2O_3.[28]

To ensure that only the chemical environments of InSb and In_2O_3 are present during the evolution of InSb semiconductor upon air aging for the In $M_{4,5}N_{4,5}N_{4,5}$ X-AES lines,

we performed a space dimension determination. The resulting abstract factors are displayed in Fig. 1 b, with two abstract factors (black and red ones) showing significant variation and the others appearing as mostly horizontal traces. Thus, it confirms that by using solely pristine InSb and In_2O_3 chemical environments, it is possible to fully describe the evolution of In $M_{4,5}N_{4,5}N_{4,5}$ X-AES lines during InSb aging.

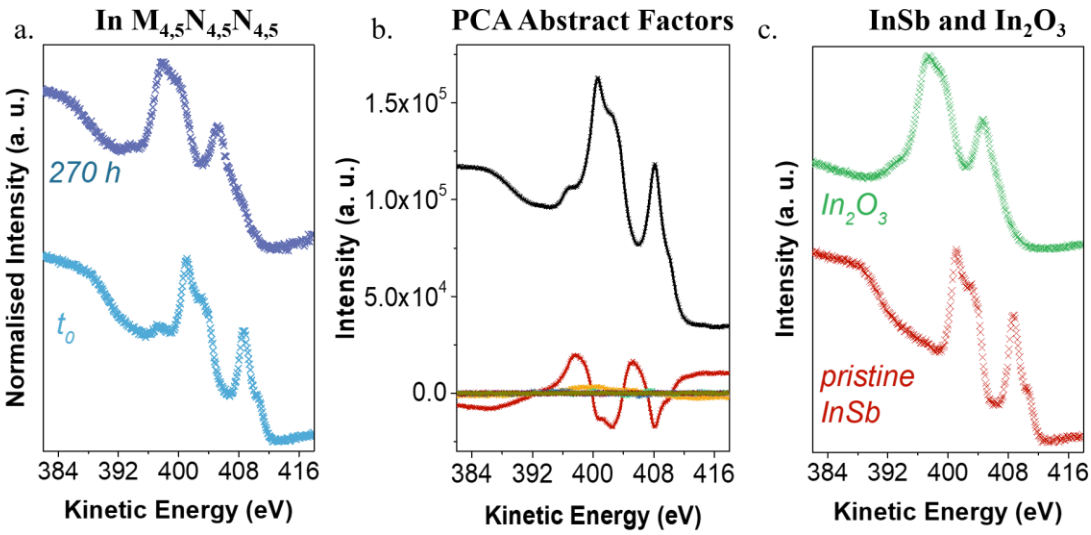

FIG. 1. In $M_{4,5}N_{4,5}N_{4,5}$ X-AES lines measured on InSb at t_0 and after 270 hours of aging in air (a.) Space dimension determination from spectra in (a.) after removing a constant intensity offset from each spectrum for InSb (b.). In $M_{4,5}N_{4,5}N_{4,5}$ X-AES transitions of InSb pristine chemical environment obtained with the vectorial method (red curve) and In_2O_3 experimental spectrum (green curve) (c.).

The subsequent stage involves accurately defining the shapes of the two chemical environments. The modified Auger parameters of t_0 and 270 hours aged InSb showed that InSb and In_2O_3 are the two main chemical environments.[14,31] To define the InSb and the

In_2O_3 In $M_{4,5}N_{4,5}N_{4,5}$ X-AES transition shapes, the vectorial method is used to calculate representative vectors for these two chemical environments.[25,26] To do this, the initial (t_0) and the final (270 hours) In $M_{4,5}N_{4,5}N_{4,5}$ X-AES lines are subtracted from each other with a weighted differentiation, using a step size of 0.1, as previously described in the literature.[25,26] A set of one hundred spectra were obtained and the identified InSb In $M_{4,5}N_{4,5}N_{4,5}$ X-AES line must be free of any oxide contribution. It was identified based on coherent physical meaning and coherent spectroscopic information (Fig. 1 c.). The In $M_4N_{4,5}N_{4,5}$ transition is found at 408.7 eV ± 0.1 eV, KE, and the In $M_5N_{4,5}N_{4,5}$ line is at 401.3 ± 0.1 eV, which is in good agreement with the original InSb X-AES spectrum.

To determine the chemical surroundings of In_2O_3, there are two possible options: using the vectorial method or an experimental In_2O_3 spectrum. Since the obtained shapes are in perfect agreement (see supplementary material at [URL will be inserted by AIP Publishing] for the comparison of the In_2O_3 experimental spectrum and the In_2O_3 vectorial spectrum, Fig. S1), the decompositions of the InSb aged X-AES transitions are performed using the In_2O_3 experimental spectrum. As for the definition of the In_2O_3 chemical environment (Fig. 1 c.), the experimental spectrum provides an In $M_4N_{4,5}N_{4,5}$ transition located at 405.8 eV ± 0.1 eV, KE, and an In $M_5N_{4,5}N_{4,5}$ line at 398.7 ± 0.1 eV, KE.

As we dispose now of reference spectra of In $M_{4,5}N_{4,5}N_{4,5}$ X-AES for the 2 chemical environments that will be detected at the surface of the InSb sample during aging, the two fitting approaches (linear and non-linear least square fitting) can be implemented.

2. Non-linear least square decompostion of the In $M_{4,5}N_{4,5}N_{4,5}$ X-AES spectra

The non-linear least square analysis strategy is firstly considered to reveal the evolution of the InSb oxidation kinetic by means of the In $M_{4,5}N_{4,5}N_{4,5}$ X-AES transition evolution. To perform this analysis, one must establish the chemical environments of InSb and In_2O_3 *via* a series of photopeaks, respecting to certain parameters such as position, FWHM values, and percentage of area, all fixed with regards to a major peak. To accurately model the In $M_{4,5}N_{4,5}N_{4,5}$ X-AES lines in In_2O_3, six contributions must be utilized. The main peak, which is representative of the In $M_4N_{4,5}N_{4,5}$ X-AES transition, is positioned at 405.6 eV. The relationships among the principal peak and the five others are described in Table 2 and the final decomposition is displayed in Fig. 2 a. For the In $M_{4,5}N_{4,5}N_{4,5}$ X-AES description of the InSb spectrum previously obtained through the vectorial method (Fig. 1 c.), nine peaks are necessary to achieve an adequate decomposition (Table 2 and Fig. 2 b.). Again, the principal peak is positioned as the major contribution to the In $M_4N_{4,5}N_{4,5}$ X-AES transition, at 408.7 eV. The discrepancy between the number of peaks describing the two X-AES lines may be attributed to the initial shape of the transitions since the In_2O_3 spectrum shows a higher FWHM value for the In $M_4N_{4,5}N_{4,5}$ X-AES transition than the InSb one (3.1 ± 0.1 eV vs 1.9 ± 0.1 eV, respectively).

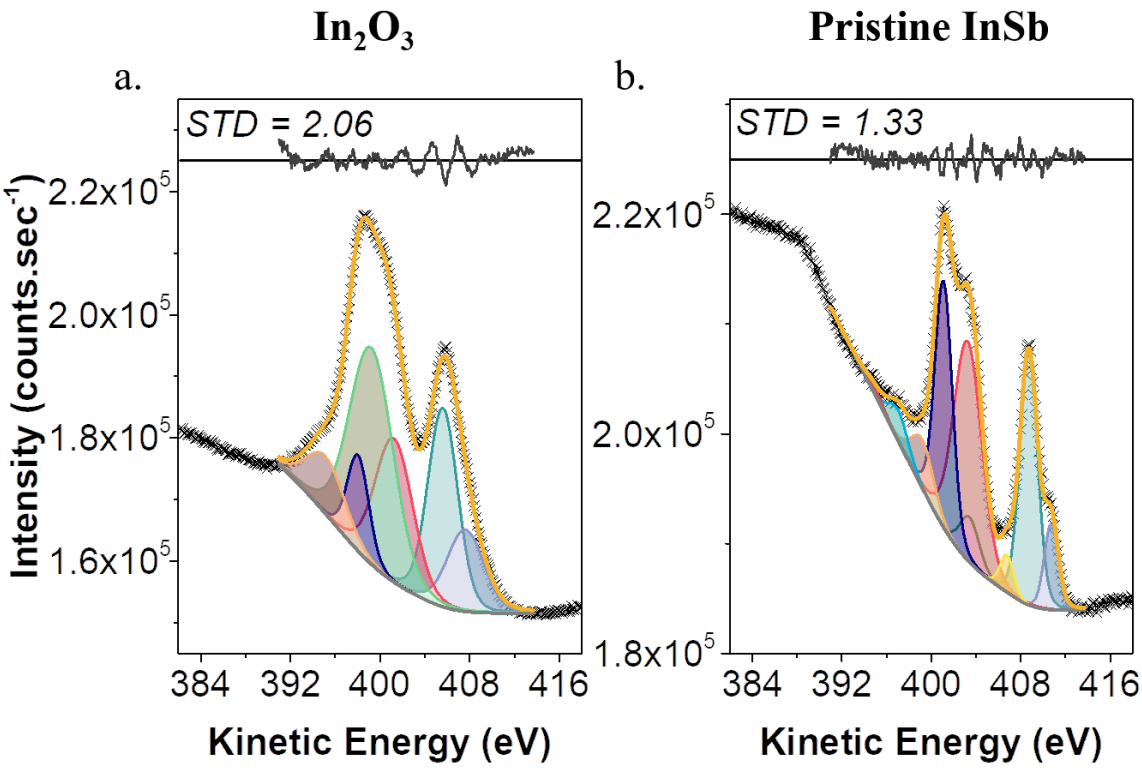

FIG 2. Non-linear modeling of the In $M_{4,5}N_{4,5}N_{4,5}$ X-AES transitions for In_2O_3 (a.) and pristine InSb (b.) with 6 and 9 arbitrary photopeaks, respectively.

TABLE 2. Parameters used for the non-linear square fit of the In $M_{4,5}N_{4,5}N_{4,5}$ X-AES transitions for In_2O_3 and InSb, with PP as the principal peak.

		Principal peak	Peak 2	Peak 3	Peak 4	Peak 5	Peak 6	Peak 7	Peak 8	Peak 9
In_2O_3	Position (eV)	405.6 ± 0.2	PP + 2.0	PP – 4.4	PP – 6.4	PP – 7.6	PP – 10.5	/	/	/
	FWHM (eV)	3.1 ± 0.1	PP * 1.22	PP* 1.26	PP * 1.46	PP * 0.72	PP * 1.30	/	/	/
	Area (%)	21.0	10.6	19.2	33.8	7.4	8.0	/	/	/
In Sb	Position (eV)	408.7 ± 0.2	PP + 2.0	PP – 5.3	PP – 5.4	PP – 7.6	PP – 9.5	PP- 1.9	PP- 11.7	PP- 13.8

FWHM (eV)	1.9 ± 0.1	PP * 0.79	PP* 1.10	PP * 1.59	PP * 0.99	PP * 1.27	PP * 0.77	PP * 1.12	PP *1.01
Area (%)	23.0	6.2	4.5	31.8	22.4	5.6	2.6	3.2	0.7

To demonstrate the changes in the oxide component within the X-AES lines as time progresses, the 15 arbitrary peaks previously determined for InSb (9 photopeaks) and In_2O_3 (6 photopeaks) are added to the experimental InSb spectrum at t_0 (Fig. 3 a.). Only the principal peaks parameters (energy position and FWHM) are allowed to slightly be modified, driving the others in a same way. See supplementary material at [URL will be inserted by AIP Publishing] (Table S1) for the positions and full width at half maximum (FWHM) values of the primary peaks of InSb and In_2O_3 chemical contributions to the fitted data for aged InSb. The reported values demonstrate an excellent stability over time when compared to the initial chemical environments.

The result of this fitting procedure shows that a significant oxide contribution is detected at t_0, leading to the hypothesis of insufficient deoxidation (23.6 at. %, within the In $M_{4,5}N_{4,5}N_{4,5}$ X-AES transition decomposition, Table 3). Additionally, the Sb 3d – O 1s region decomposition (see supplementary material at [URL will be inserted by AIP Publishing] for the curves fitted to data of the Sb 3d - O 1s region (a.) and C 1s (b.) photopeak at t_0., Fig. S2.) confirms the presence of an oxide contribution at the initial stage, in particular with an oxide contribution to the O 1s signal at 529.9 ± 0.1 eV, BE. A carbonaceous contamination layer is also identifiable with the C 1s signature associated to the O 1s contribution at 532.5 ± 0.1 eV, BE. As the aging progresses, the oxide contribution increases (Fig. 3 b. and Table 3), and the In_2O_3 contribution becomes predominant after 150 hours of aging. See supplementary material at [URL will be inserted by AIP

Publishing] (Fig. S3) for the evolution of the In $M_{4,5}N_{4,5}N_{4,5}$ transitions for InSb using non-linear least square decomposition for 30 min, 1 hour, 3 hours and 4 hours. Eventually, the percentage of oxide reaches as high as 92.2% at the end of aging.

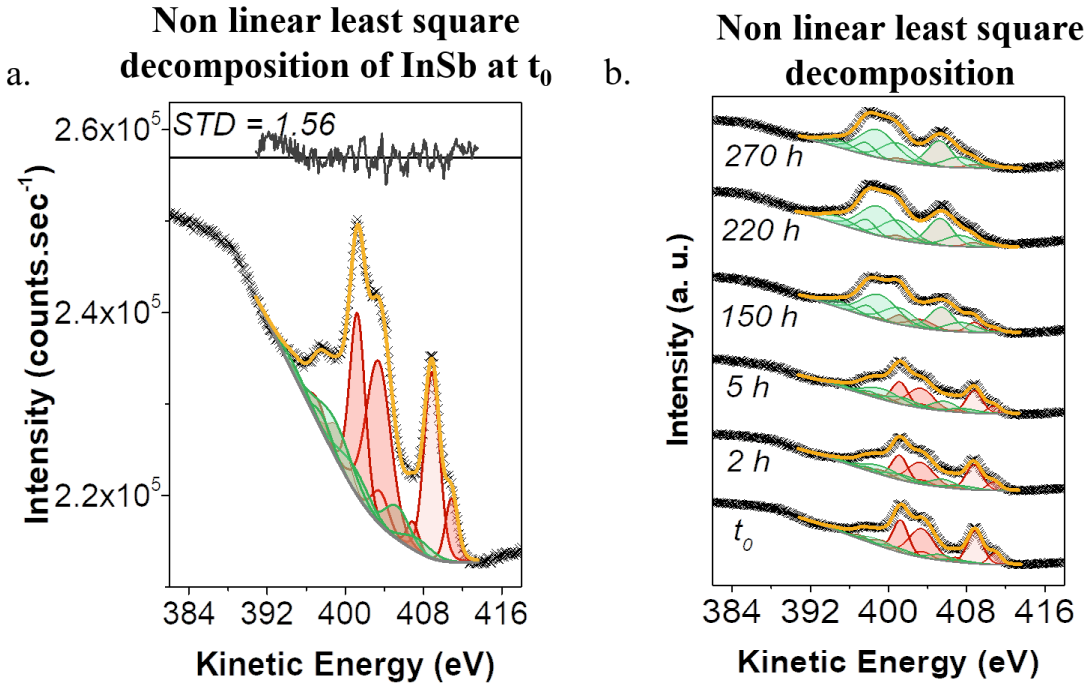

FIG. 3. Non-linear decomposition of the experimental In $M_{4,5}N_{4,5}N_{4,5}$ line of InSb at t_0 (a.) and Evolution of the non-linear least square decomposition of In $M_{4,5}N_{4,5}N_{4,5}$ transitions for InSb for different aging times (b.). with the InSb and the In_2O_3 chemical environments in red and green, respectively.

3. Linear least square decomposition of the In $M_{4,5}N_{4,5}N_{4,5}$ X-AES spectra

The other alternative method to perform the X-AES decomposition is the linear least square approach. This method entails in a linear analysis that mathematically

combines directly the pristine InSb spectrum defined by the vectorial method and the experimental In_2O_3 spectrum (Fig. 1 c.). It allows the curves to be fitted to data of the X-AES lines of In $M_{4,5}N_{4,5}N_{4,5}$ over time but prohibits any modification in terms of FWHM constraints.

Using a U 2 Tougaard background, the decomposition of the In $M_{4,5}N_{4,5}N_{4,5}$ transition at t_0 is performed, and, as for the non-linear decomposition, two chemical environments are mandatory: the pristine InSb spectral shape and the In_2O_3 one, with a 24.2 at. % of oxide contribution (Fig. 4 a., Table 3), in agreement with previous results obtained with the non-linear decomposition. Further aging of InSb in air (Fig. 4 b.) results in an incremental rise of the In_2O_3 phase within the decomposition of the In $M_{4,5}N_{4,5}N_{4,5}$ X-AES transitions. This is evident from the data displayed in Table 3, with the oxide percentage increasing to 45.8 at.% after 5 hours of aging and up to 94.7 at.% after 270 hours. See supplementary material at [URL will be inserted by AIP Publishing] (Fig. S4) for the evolution of the In $M_{4,5}N_{4,5}N_{4,5}$ transitions for InSb using linear least square decomposition for 30 min, 1 hour, 3 hours and 4 hours.

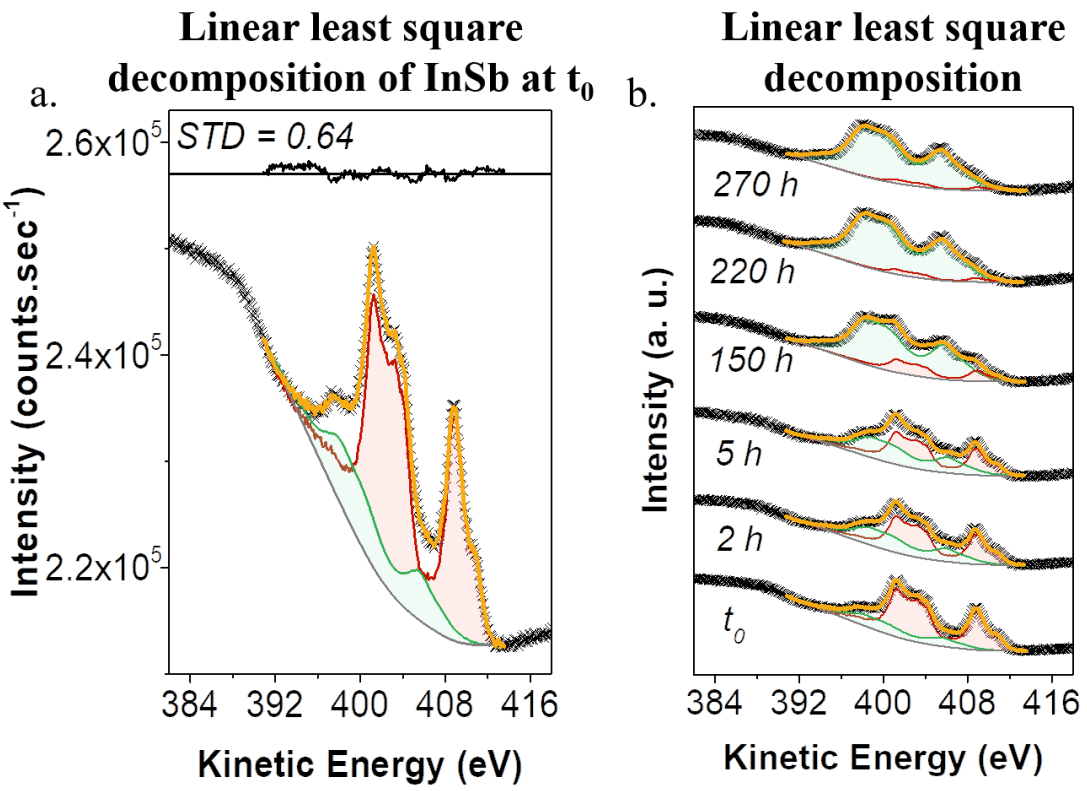

FIG. 4. Linear decomposition of the experimental In $M_{4,5}N_{4,5}N_{4,5}$ line of aged InSb at t_0 (a.). Evolution of the linear least square decomposition of In $M_{4,5}N_{4,5}N_{4,5}$ transitions for InSb using for different aging times (b.). The InSb and the In_2O_3 chemical environments are shown in red and green, respectively.

The comparison between the non-linear and the linear least square decompositions can be made by assessing the difference in oxide contribution for each aging time (Table 3). The two decomposition methods exhibit good agreement as there are relative errors ranging from 2.1% to 9.2% maximum over the ten spectra fitted during the aging process.

The thickness of the In_2O_3 oxide covering the InSb semiconductor increases gradually (Table 3, oxide thickness calculated based on Equation 2). Based on In $M_{4,5}N_{4,5}N_{4,5}$ X-AES transitions interpretation, at the end of the aging, the InSb

semiconductor is covered with a 2.7 ± 0.2 nm oxide layer. This is coherent with the evaluated probing depth of 3 to 4 nm and the fact that InSb chemical environment is still detected (Table 3).

TABLE 3**.** Percentage evolution of the oxide contribution calculated from the area of the In oxide contribution to the total In $M_{4,5}N_{4,5}N_{4,5}$ X-AES transitions obtained with non-linear and linear fits. Oxide thickness values on the InSb aged sample for the In $M_{4,5}N_{4,5}N_{4,5}$ X-AES transitions are calculated according to Equation 2. Relative errors between non-linear and linear fittings are obtained according to the following formula:

$$\frac{\left|at.\%\ In_{ox_{non\ linear}} - at.\ \%\ In_{ox_{linear}}\right|}{at.\%\ In_{ox_{minimum}}}.$$

		0 hours	30 min	1 hour	2 hours	3 hours	4 hours	5 hours	150 hours	220 hours	270 hours
Oxide atomic percentage	Non-linear fitting	23.7	30.0	35.4	35.6	35.7	40.4	42.2	80.2	91.2	92.2
	Linear fitting	24.2	32.2	34.0	37.3	39.0	43.3	45.8	82.6	93.7	94.7
Relative error		2.1%	7.3%	4.1%	4.7%	9.2%	7.2%	8.5%	3.0%	2.7%	2.7%
Oxide thickness (nm) (± 0.2 nm)	Non-linear fitting	0.3	0.4	0.5	0.5	0.5	0.5	0.6	1.6	2.4	2.5
	Linear fitting	0.3	0.4	0.4	0.5	0.5	0.6	0.6	1.7	2.7	2.9

B. Oxidation comparison between X-AES lines and XPS photopeaks during air aging

1. In 3d and In 4d photopeaks comparison

A comparative study using In photopeaks at lower kinetic energies is also conducted to evaluate the impact of the escape depth. Indeed, the In 3d electrons and the In 4d electrons, which escape with 1042 eV, KE (444.5 eV, BE) and 1470 eV, KE (17.5 eV, BE) are representative of a probed thickness until 6 to 10 nm and should be less affected by oxidation. Thus, a non-linear least square method is used to investigate the subsurface evolution of In in order to demonstrate the significance of oxidation as a function of the probed depth.

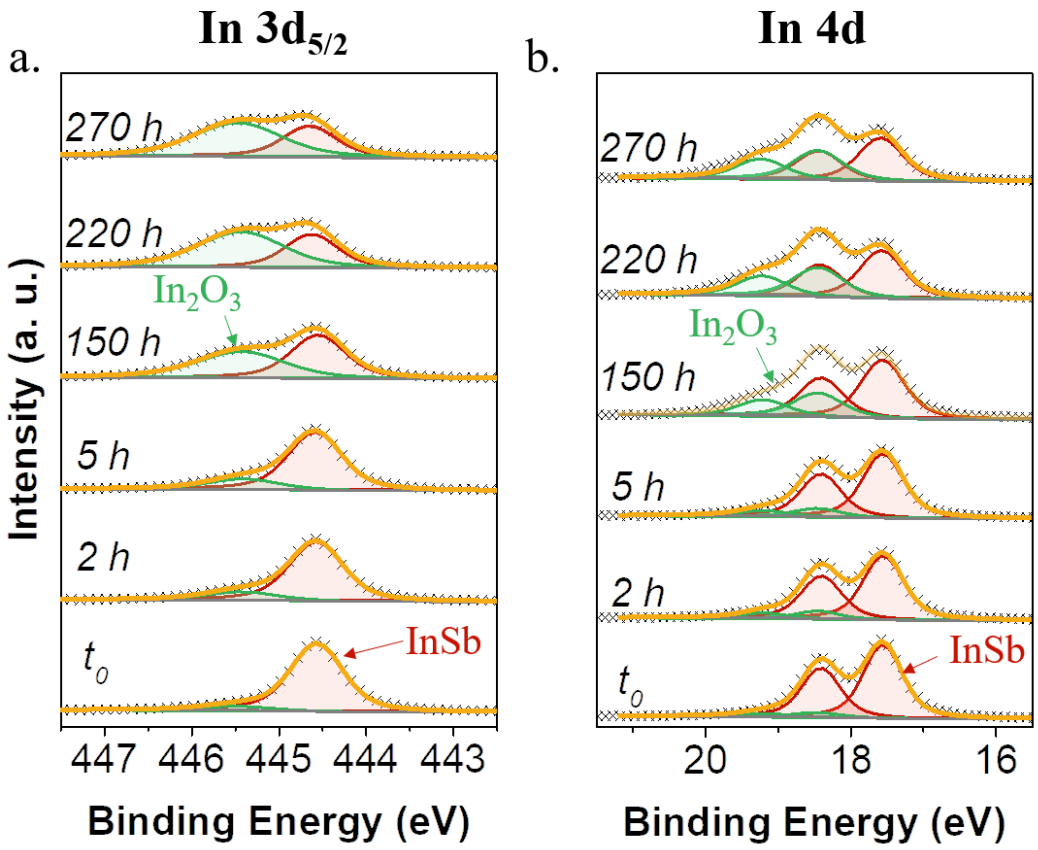

FIG 5. Curves fitted to data of In $3d_{5/2}$ (a.) and In 4d (b.) spectra during air aging for InSb. The red contributions are representative of the non-oxidized environment and the green ones of the oxidized one.

Fig. 5 a. illustrates the curves fitted to the data of InSb during air aging for In $3d_{5/2}$. For further details on the fitting parameters, See supplementary material at [URL will be inserted by AIP Publishing] (Table S2) for the parameter fits for the In $3d_{5/2}$ photopeak during air aging. At t_0, two chemical environments are noticeable. The first one is related to InSb, with a position at 444.6 eV ± 0.1 eV, BE, and a FWHM value of 0.72 ± 0.05 eV. The second one pertains to an In_2O_3 oxide phase, with a position at 445.5 ± 0.1 eV, BE, and a FWHM value of 0.90 ± 0.05 eV. The presence of the second chemical environment reinforces the results obtained for the In $M_{4,5}N_{4,5}N_{4,5}$ X-AES transitions, showing a poor deoxidation of the InSb semiconductor. At t_0, the decomposition of the $In3d_{5/2}$ photopeak leads to an oxide content of 7.0% (Table 4). During the five first hours of air aging, the In_2O_3 contribution increases to attain an In_2O_3 percentage of 18.9% after 5 hours of aging. As soon as more than 150 hours of air aging are performed, the percentage evolves up to 49.0% and is accompanied by an increase in the FWHM parameter (from 0.95 to 1.19 eV) which is related to an amorphization of the substrate due to the presence of the oxide layer.[32] As the aging continues, the contribution of oxide keeps on increasing, indicating a gradual alteration of the chemical environment and finally hitting 64.2 % after 270 hours of aging. This is also consistent with the overall atomic composition shown in supplementary material at [URL will be inserted by AIP Publishing] (Table S3, atomic composition based on C 1s, In $3d_{5/2}$, Sb $3d_{5/2}$ and O 1s photopeaks). After the aging process, the thickness of the oxide within the 6-8 nm depth range was found to be 2 ± 0.2 nm. This was determined by analyzing the oxide contribution in the In $3d_{5/2}$ photopeak.

Fig. 5 b. illustrates the evolution of the In 4d photopeaks with air aging for InSb. The 4d photopeak exhibits two chemical environments at t_0, as seen in the X-AES lines and in the $3d_{5/2}$ photopeak. One environment relates to InSb (In $4d_{5/2}$ at 17.6 eV, BE with a FWHM value of 0.63 ± 0.05 eV) while the other relates to In_2O_3 (In $4d_{5/2}$ at 18.5 eV, BE, FWHM value of 0.75 ± 0.05 eV), leading to a percentage of oxide (within the In $4d_{5/2}$ decomposition) of 6.7 % (Table 4). The contribution of oxide continues to increase during aging, with a turning point after 150 hours of aging: the oxide percentage doubles (from 12.5 % after 5 hours to 31.3% after 150 hours). See the supplementary material at [URL will be inserted by AIP Publishing] (Table S4) for the parameter fits for the In $4d_{5/2}$ photopeak during air aging. Moreover, there is a corresponding escalation in the FWHM values, consistent with the theory of InSb surface amorphization, as stated in detail for the decomposition of the In $3d_{5/2}$ photopeak. The oxide percentage steadily increased until it reached the ultimate value of 42.6%, resulting in an oxide thickness of 2 ± 0.2 nm for the 7-10 nm depth scanned for the In 4d photopeak.

Similar trends are observed for both In $3d_{5/2}$ and In 4d photopeaks, with a progressive increase in the oxide content, and an enlargement of the FWHM value due to amorphization. However, the amount of oxide detected in In 4d is slightly less than that in In $3d_{5/2}$ one, because of the electrons' escaping depth. Nevertheless, these two photopeaks are probed to the same depths (between 8 and 10 nm for InSb), which results in very similar oxide thicknesses on top of the InSb semiconductor throughout the aging process.

TABLE 4. Percentage of oxide contribution evolution calculated from the area of the In_2O_3 contribution over the InSb contribution for the In $3d_{5/2}$ and In $4d_{5/2}$ photopeaks of InSb.

Oxide thickness values on the InSb aged sample for the In $3d_{5/2}$ and In $4d_{5/2}$ photopeaks are calculated according to Equation 2.

		0 hours	30 min	1 hour	2 hours	3 hours	4 hours	5 hours	150 hours	220 hours	270 hours
Oxide atomic percentage	In $3d_{5/2}$	7.0	11.3	13.7	15.4	17.0	18.7	18.9	49.0	63.0	64.2
	In $4d_{5/2}$	6.7	8.3	9.6	10.8	11.3	12.1	12.5	31.3	40.4	42.6
Oxide thickness (nm) (± 0.2 nm)	In $3d_{5/2}$	0.2	0.2	0.3	0.3	0.4	0.4	0.4	1.4	2.0	2.0
	In $4d_{5/2}$	0.2	0.2	0.3	0.3	0.3	0.3	0.4	1.0	1.4	1.5

As expected, oxidation has a greater impact on the photoelectrons originating from the In $M_{4,5}N_{4,5}N_{4,5}$ X-AES lines compared to the In 3d and In 4d photopeaks, considering their lower escape depth. With aging, the oxide contributions penetrate progressively into the InSb semiconductor, as illustrated in Fig. 6. As a result, the oxide thickness becomes more important with time.

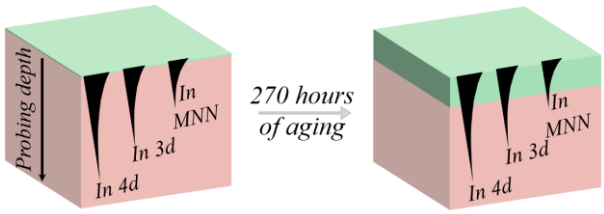

FIG. 6. Schematic evolution of the growth of the oxide (green part) over the InSb semiconductor (pink layer), according to the probing depth and the different X-AES transitions and photopeaks used.

2. Sb 3d and Sb 4d photopeaks comparison

In addition to analyzing the indium chemical environment, we also investigate the antimony environment, using Sb 3d and Sb 4d photopeaks. Indeed, previous studies have shown that the InSb binary compound produces two distinct oxides during aging, each corresponding to one of its elements, rather than a mixture.[14,33] As for In 3d and In 4d, the escape depths of these electrons result in probed thicknesses ranging from 6 to 10 nm.

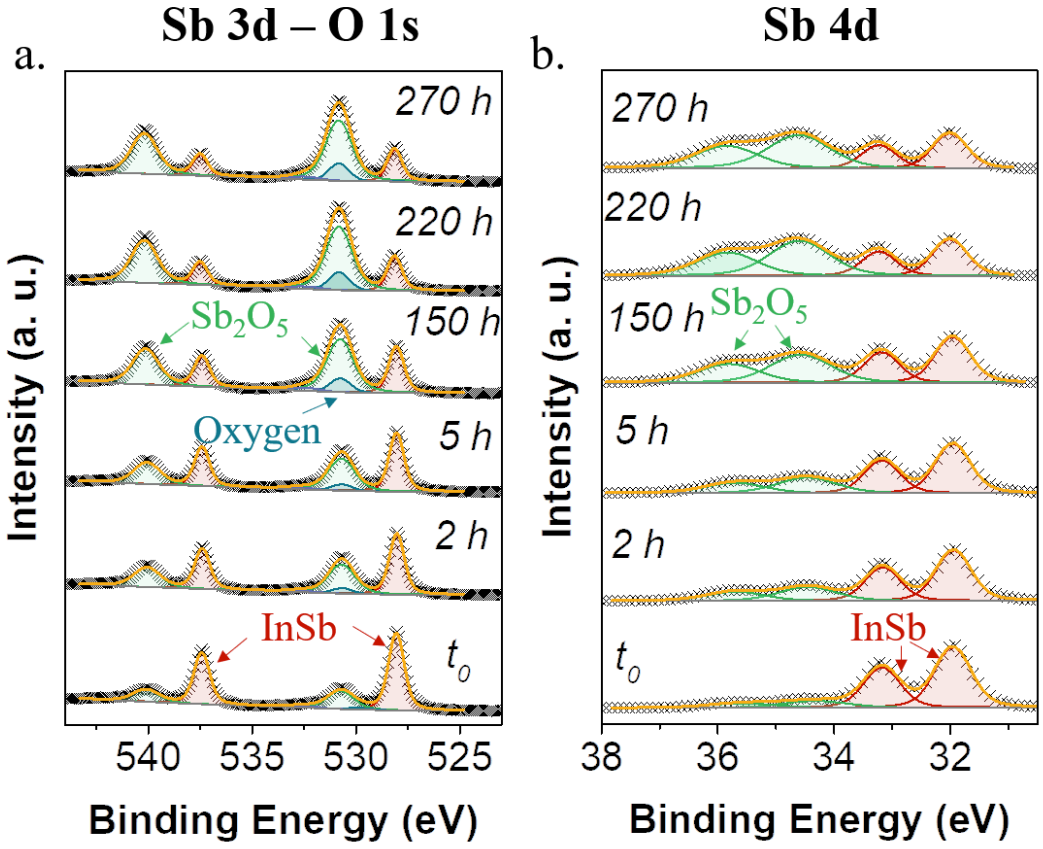

FIG. 7. Curves fitted to data of Sb 3d (a.) and Sb 4d (b.) spectra during air aging for InSb. The red contributions are representative of the non-oxidized environment and the green ones of the oxidized one.

Fig. 7 a. displays the evolution of the Sb 3d region, superimposed with the O 1s contribution (See the supplementary material at [URL will be inserted by AIP Publishing] (Table S5) for the parameter fits for the Sb 3d – O 1s region during air aging). As for indium, two chemical environments are discernible at t_0, one for InSb with the Sb $3d_{5/2}$ photopeak positioned at 528.1 ± 0.1 eV and the other related to the oxide phase Sb_2O_5 at 530.7 ± 0.1 eV, as corroborated by the literature,[14,33] inducing a Sb_2O_5 oxide thickness of 1.1 ± 0.2 nm (TABLE 5). Over time, the oxide contribution continues to increase until it reaches a final thickness of 4.1 ± 0.2 nm.

The decomposition of the Sb 4d region (Fig. 7 b. and supplementary material at [URL will be inserted by AIP Publishing] (Table S6) for the parameter fits for the Sb 4d region during air aging) provides similar results, with at t0, the InSb chemical environment located at 31.9 ± 0.1 eV and the Sb_2O_5 one at 34.3 ± 0.1 eV. This provides an oxide with a thickness of 0.9 ± 0.2 nm which keeps on rising up to 4.0 ± 0.2 nm after the 270 hours of aging (TABLE 5).

TABLE 5. Percentage of oxide contribution evolution calculated from the area of the Sb_2O_5 contribution over the InSb contribution for the Sb $3d_{5/2}$ and Sb $4d_{5/2}$ photopeaks of InSb. Oxide thickness values on the InSb aged sample for the Sb $3d_{5/2}$ and Sb $4d_{5/2}$ photopeaks are calculated according to Equation 2.

		0 hours	30 min	1 hour	2 hours	3 hours	4 hours	5 hours	150 hours	220 hours	270 hours
Oxide atomic percentage	Sb $3d_{5/2}$	28.2	40.5	44.1	45.9	47.7	48.0	49.5	67.2	77.5	77.7
	Sb $4d_{5/2}$	17.3	26.4	29.6	31.2	32.6	33.3	34.3	51.4	62.6	62.9
Oxide thickness	Sb $3d_{5/2}$	1.1	1.7	1.8	1.9	2.0	2.0	2.1	3.2	4.1	4.1

Sb $4d_{5/2}$	0.9	1.4	1.6	1.7	1.8	1.8	1.9	3.0	4.0	4.0

A difference in thickness is observed between the two oxide layers, with the Sb_2O_5 layer being thicker than the In_2O_3 layer for similar probed thicknesses. This can be attributed to the difference in oxidation kinetics noted in literature,[33] as well as an inadequate initial deoxidation step.

IV. SUMMARY AND CONCLUSIONS

In this paper, we highlight the benefit of utilizing X-AES transitions and present two distinct methodologies for examining the evolution of In_2O_3 oxide growth on InSb substrates. We have applied non-linear and linear least squares analyses on multiple photopeaks and X-AES transitions of indium to achieve this objective. The results demonstrate the progressive oxidation front.

The vectorial method was employed to perform decompositions on the In $M_{4,5}N_{4,5}N_{4,5}$ X-AES transitions. This method helped define two chemical environments: a deoxidized and an oxidized environment. These environments were used to describe the chemical evolution of the In $M_{4,5}N_{4,5}N_{4,5}$ X-AES lines. Nonlinear and linear least squares fits were used to study the decomposition of In $M_{4,5}N_{4,5}N_{4,5}$ X-AES transitions. We demonstrate that both methods exhibit a robust correlation, can be readily replicated on similar intricate datasets, encompassing other X-AES transitions, but have their respective advantages and limitations. The non-linear approach initially appears straightforward for complex data analysis. Nevertheless, the model relies on numerous contributions (corresponding with the number of chemical contexts), which could introduce potential errors when applied to the fit. When utilized on a developed dataset, slight adjustments are

possible, such as increasing the full width at half maximum (FWHM) values. On the contrary, if the linear least squares approach does not allow for any modification of the initial shape implemented, there should be no specific errors encountered when reported to the fit.

The combined use of non-linear and linear least square analysis and all available photoemission transitions expands the explored kinetic energy range, enabling more precise determination of the evolution of material chemical environments from the outer surface to the subsurface. Specifically, the results highlight the uniform growth of an In_2O_3 layer over the InSb substrate.

SUPPLEMENTAL MATERIAL

See supplementary material at [URL will be inserted by AIP Publishing] for the comparison of the In_2O_3 experimental X-AES spectrum and the In_2O_3 vector obtained by the vectorial method; the table of parameters decomposition for the X-AES non-linear least square decomposition; the curves fitted to data of the Sb 3d - O 1s region and C 1s photopeak at t_0; the evolution of the In $M_{4,5}N_{4,5}N_{4,5}$ transitions for InSb using non-linear least square decomposition for 30 min, 1 hour, 3 hours and 4 hours; the evolution of the In $M_{4,5}N_{4,5}N_{4,5}$ transitions for InSb using linear least square decomposition for 30 min, 1 hour, 3 hours and 4 hours; the parameter fits for the In $3d_{5/2}$ photopeak during air aging; the atomic percentages during air aging calculated from the C 1s, In $3d_{5/2}$, Sb $3d_{5/2}$ and O 1s photopeaks; the parameter fits for the In $4d_{5/2}$ photopeak during air aging; the parameter fits for the Sb $3d_{5/2}$ photopeak during air aging; the parameter fits for the Sb $4d_{5/2}$ photopeak during air aging.

ACKNOWLEDGMENTS

S. Bechu thanks M. Bouttemy, M. Fregnaux, D. Aureau, and M. Al Katrib for the fruitful discussions.

AUTHOR DECLARATIONS

Conflicts of Interest

The authors have no conflicts to disclose.

Author Contributions *(if applicable)*

Solene Bechu: Conceptualization, Methodology, Investigation, Formal Analysis, Writing – Original Draft. **Neal Fairley**: Software, Methodology, Formal Analysis, Writing – Original Draft.

DATA AVAILABILITY

The data that supports the findings of this study are available within the article [and its supplementary material].

REFERENCES

[1] M. Bosi and C. Pelosi, Prog. Photovoltaics Res. Appl. **15**, 51 (2007).

[2] K. Tanabe, Energies 2009, Vol. 2, Pages 504-530 **2**, 504 (2009).

[3] S. Mokkapati and C. Jagadish, Mater. Today **12**, 22 (2009).

[4] A. Gocalinska, S. Rubini, and E. Pelucchi, Appl. Surf. Sci. **383**, 19 (2016).

[5] S.B. Donald, Z.R. Dai, M.L. Davisson, J.R. Jeffries, and A.J. Nelson, J. Nucl. Mater. **487**, 105 (2017).

[6] G. Bridoux, G.D. Ruano, J.M. Ferreyra, and M. Villafuerte, J. Appl. Phys. **127**, 245704 (2020).

[7] S. Béchu, M. Bouttemy, J. Guillemoles, and A. Etcheberry, Appl. Surf. Sci. **576**, 151898 (2022).

[8] C.S. Fadley, Prog. Surf. Sci. **16**, 275 (1984).

[9] C.D. Wagner and A. Joshi, J. Electron Spectros. Relat. Phenomena **47**, 283 (1988).

[10] M. Bedrouni, B. Kharroubi, A. Ouerdane, M. Bouslama, M. Guezzoul, Y. Caudano, K.B. Bensassi, M. Bousmaha, M.A. Bezzerrouk, A. Mokadem, and M. Abdelkrim, Opt. Mater. (Amst). **111**, 110560 (2021).

[11] P. Northover, A. Crossley, C. Grazioli, N. Zema, S. La Rosa, L. Lozzi, P. Picozzi, and E. Paparazzo, Surf. Interface Anal. **40**, 464 (2008).

[12] N. Nicoara, S. Harel, T. Lepetit, L. Arzel, N. Barreau, and S. Sadewasser, ACS Appl. Energy Mater. **1**, 2681 (2018).

[13] S. Harel, L. Arzel, T. Lepetit, P. Zabierowski, and N. Barreau, ACS Appl. Mater. Interfaces **12**, 46953 (2020).

[14] H. Iwasaki, Y. Mizokawa, R. Nishitani, and S. Nakamura, Surf. Sci. **86**, 811 (1979).

[15] M.C. Biesinger, Surf. Interface Anal. **49**, 1325 (2017).

[16] J.J. Moré, Numer. Anal. **630**, 105 (1978).

[17] N. Fairley, V. Fernandez, M. Richard-Plouet, C. Guillot-Deudon, J. Walton, E. Smith, D. Flahaut, M. Greiner, M. Biesinger, S. Tougaard, D. Morgan, and J. Baltrusaitis, Appl. Surf. Sci. Adv. **5**, 100112 (2021).

[18] G.H. Golub and C. Reinsch, Linear Algebr. **420**, 403 (1971).

[19] B.M. Garland, N. Fairley, N.C. Strandwitz, R. Thorpe, P. Bargiela, and J. Baltrusaitis, Appl. Surf. Sci. **598**, 153827 (2022).

[20] R.A. Gilbert, J.A. Llewellyn, W.E. Swartz, and J.W. Palmer, Appl. Spectrosc. **36**, 428 (1982).

[21] M.F. Koenig and J.T. Grant, J. Electron Spectros. Relat. Phenomena **41**, 145 (1986).

[22] J. Zhou, K. Varazo, J.E. Reddic, M.L. Myrick, and D.A. Chen, Anal. Chim. Acta **496**, 289 (2003).

[23] K. Sakamoto, F. Hayashi, K. Sato, M. Hirano, and N. Ohtsu, Appl. Surf. Sci. **526**, 146729 (2020).

[24] B.M. Garland, N. Fairley, N.C. Strandwitz, R. Thorpe, P. Bargiela, and J. Baltrusaitis, Appl. Surf. Sci. **598**, (2022).

[25] J. Baltrusaitis, B. Mendoza-Sanchez, V. Fernandez, R. Veenstra, N. Dukstiene, A. Roberts, and N. Fairley, Appl. Surf. Sci. **326**, 151 (2015).

[26] S. Béchu, B. Humbert, V. Fernandez, N. Fairley, and M. Richard-Plouet, Appl. Surf. Sci. **447**, 528 (2018).

[27] G. Greczynski and L. Hultman, Prog. Mater. Sci. **107**, 100591 (2020).

[28] A. V. Naumkin, A. Kraut-Vass, S.W. Gaarenstroom, and C.J. Powell, (2012).

[29] T.A. Carlson and G.E. McGuire, J. Electron Spectros. Relat. Phenomena **1**, 161 (1972).

[30] B.R. Strohmeier, Surf. Interface Anal. **15**, 51 (1990).

[31] W.K. Liu and M.B. Santos, J. Vac. Sci. Technol. B Microelectron. Nanom. Struct. Process. Meas. Phenom. **14**, 647 (1996).

[32] S. Béchu, A. Loubat, M. Bouttemy, J. Vigneron, J.-L. Gentner, and A. Etcheberry, Thin Solid Films **669**, 425 (2019).

[33] X. Tang, R.G. Van Welzenis, F.M. Van Setten, and A.J. Bosch, Semicond. Sci. Technol. **1**, 355 (1986).

TABLES

TABLE 1. IMFP values for the different chemical environments.

KE of emitted photoelectrons (eV)	Transition	λ_{InSb} (Å)	$\lambda_{In_2O_3}$ (Å)	$\lambda_{Sb_2O_5}$ (Å)	InSb depth probed (nm)	In_2O_3 depth probed (nm)	Sb_2O_5 depth probed (nm)	$N_{In_2O_3}$	N_{InSb}	$N_{Sb_2O_5}$
1468	In 4d	33.88	24.04	/	10	7	/	7.18	5.78	/
1042	In $3d_{5/2}$	25.93	18.50	/	8	6	/			
408	In $M_4N_{4,5}N_{4,5}$	13.10	9.52	/	4	3	/			
1454	Sb 4d	33.67	/	28.45	10	/	9	/		3.78
958	Sb $3d_{5/2}$	24.38	/	20.54	7	/	6			

TABLE 2. Parameters used for the non-linear square fit of the In $M_{4,5}N_{4,5}N_{4,5}$ X-AES transitions for In_2O_3 and InSb, with PP as the principal peak.

		Principal peak	Peak 2	Peak 3	Peak 4	Peak 5	Peak 6	Peak 7	Peak 8	Peak 9
In_2O_3	Position (eV)	405.6 ± 0.2	PP + 2.0	PP – 4.4	PP – 6.4	PP – 7.6	PP – 10.5	/	/	/
	FWHM (eV)	3.1 ± 0.1	PP * 1.22	PP* 1.26	PP * 1.46	PP * 0.72	PP * 1.30	/	/	/
	Area (%)	21.0	10.6	19.2	33.8	7.4	8.0	/	/	/
InSb	Position (eV)	408.7 ± 0.2	PP + 2.0	PP – 5.3	PP – 5.4	PP – 7.6	PP – 9.5	PP-1.9	PP-11.7	PP-13.8
	FWHM (eV)	1.9 ± 0.1	PP * 0.79	PP* 1.10	PP * 1.59	PP * 0.99	PP * 1.27	PP * 0.77	PP * 1.12	PP *1.01
	Area (%)	23.0	6.2	4.5	31.8	22.4	5.6	2.6	3.2	0.7

TABLE 3. Percentage evolution of the oxide contribution calculated from the area of the In oxide contribution to the total In $M_{4,5}N_{4,5}N_{4,5}$ X-AES transitions obtained with non-linear and linear fits. Oxide thickness values on the InSb aged sample for the In $M_{4,5}N_{4,5}N_{4,5}$ X-AES transitions are calculated according to Equation 2. Relative errors between non-linear and linear fittings are obtained according to the following formula:

$$\frac{\left|at.\%\ In_{ox_{non\ linear}} - at.\ \%\ In_{ox_{linear}}\right|}{at.\%\ In_{ox_{minimum}}}.$$

		0 hours	30 min	1 hour	2 hours	3 hours	4 hours	5 hours	150 hours	220 hours	270 hours
Oxide atomic percentage	Non-linear fitting	23.7	30.0	35.4	35.6	35.7	40.4	42.2	80.2	91.2	92.2
	Linear fitting	24.2	32.2	34.0	37.3	39.0	43.3	45.8	82.6	93.7	94.7
Relative error		2.1%	7.3%	4.1%	4.7%	9.2%	7.2%	8.5%	3.0%	2.7%	2.7%
Oxide thickness (nm) (± 0.2 nm)	Non-linear fitting	0.3	0.4	0.5	0.5	0.5	0.5	0.6	1.6	2.4	2.5
	Linear fitting	0.3	0.4	0.4	0.5	0.5	0.6	0.6	1.7	2.7	2.9

TABLE 4. Percentage of oxide contribution evolution calculated from the area of the In_2O_3 contribution over the InSb contribution for the In $3d_{5/2}$ and In $4d_{5/2}$ photopeaks of InSb. Oxide thickness values on the InSb aged sample for the In $3d_{5/2}$ and In $4d_{5/2}$ photopeaks are calculated according to Equation 2.

		0 hours	30 min	1 hour	2 hours	3 hours	4 hours	5 hours	150 hours	220 hours	270 hours
Oxide atomic percentage	In $3d_{5/2}$	7.0	11.3	13.7	15.4	17.0	18.7	18.9	49.0	63.0	64.2
	In $4d_{5/2}$	6.7	8.3	9.6	10.8	11.3	12.1	12.5	31.3	40.4	42.6
Oxide thickness (nm) (± 0.2 nm)	In $3d_{5/2}$	0.2	0.2	0.3	0.3	0.4	0.4	0.4	1.4	2.0	2.0
	In $4d_{5/2}$	0.2	0.2	0.3	0.3	0.3	0.3	0.4	1.0	1.4	1.5

TABLE 5. Percentage of oxide contribution evolution calculated from the area of the Sb_2O_5 contribution over the InSb contribution for the Sb $3d_{5/2}$ and Sb $4d_{5/2}$ photopeaks of InSb. Oxide thickness values on the InSb aged sample for the Sb $3d_{5/2}$ and Sb $4d_{5/2}$ photopeaks are calculated according to Equation 2.

		0 hours	30 min	1 hour	2 hours	3 hours	4 hours	5 hours	150 hours	220 hours	270 hours
Oxide atomic percentage	Sb $3d_{5/2}$	28.2	40.5	44.1	45.9	47.7	48.0	49.5	67.2	77.5	77.7
	Sb $4d_{5/2}$	17.3	26.4	29.6	31.2	32.6	33.3	34.3	51.4	62.6	62.9
Oxide thickness (nm) (± 0.2 nm)	Sb $3d_{5/2}$	1.1	1.7	1.8	1.9	2.0	2.0	2.1	3.2	4.1	4.1
	Sb $4d_{5/2}$	0.9	1.4	1.6	1.7	1.8	1.8	1.9	3.0	4.0	4.0

FIGURE CAPTIONS

FIG. 1. In $M_{4,5}N_{4,5}N_{4,5}$ X-AES lines measured on InSb at t_0 and after 270 hours of aging in air (a.) Space dimension determination from spectra in (a.) after removing a constant intensity offset from each spectrum for InSb (b.). In $M_{4,5}N_{4,5}N_{4,5}$ X-AES transitions of InSb pristine chemical environment obtained with the vectorial method (red curve) and In_2O_3 experimental spectrum (green curve) (c.).

FIG. 2. Non-linear modeling of the In $M_{4,5}N_{4,5}N_{4,5}$ X-AES transitions for In_2O_3 (a.) and pristine InSb (b.) with 6 and 9 arbitrary photopeaks, respectively.

FIG. 3. Non-linear decomposition of the experimental In $M_{4,5}N_{4,5}N_{4,5}$ line of InSb at t_0 (a.) and Evolution of the non-linear least square decomposition of In $M_{4,5}N_{4,5}N_{4,5}$ transitions for InSb for different aging times (b.). with the InSb and the In_2O_3 chemical environments in red and green, respectively.

FIG. 4. Linear decomposition of the experimental In $M_{4,5}N_{4,5}N_{4,5}$ line of aged InSb at t_0 (a.). Evolution of the linear least square decomposition of In $M_{4,5}N_{4,5}N_{4,5}$ transitions for InSb using for different aging times (b.). The InSb and the In_2O_3 chemical environments are shown in red and green, respectively.

FIG. 5. Curves fitted to data of In $3d_{5/2}$ (a.) and In 4d (b.) spectra during air aging for InSb. The red contributions are representative of the non-oxidized environment and the green ones of the oxidized one.

FIG. 6. Schematic evolution of the growth of the oxide (green part) over the InSb semiconductor (pink layer), according to the probing depth and the different X-AES transitions and photopeaks used.

FIG. 7. Curves fitted to data of Sb 3d (a.) and Sb 4d (b.) spectra during air aging for InSb. The red contributions are representative of the non-oxidized environment and the green ones of the oxidized one.